

SeaWinds Validation: Effect of Rain as Observed by East Coast Radars

ROSS N. HOFFMAN, CHRISTOPHER GRASSOTTI, AND S. MARK LEIDNER

Atmospheric and Environmental Research, Inc., Lexington, Massachusetts

(Manuscript received 23 December 2003, in final form 2 April 2004)

ABSTRACT

To examine the accuracy of the SeaWinds scatterometer wind data and rain flags, and how this accuracy depends on ground-based radar-estimated rain rate, SeaWinds data, WSI NEXRAD precipitation rates, and selected Eta analysis variables are collocated. [SeaWinds is the NASA scatterometer on the QuikSCAT and Advanced Earth Observing Satellite (ADEOS)-2 satellites, WSI NEXRAD precipitation data are from a Weather Services International Corporation product based on the U.S. Next Generation Radar (NEXRAD) network of Weather Surveillance Radar-1988 Doppler (WSR-88D) installations, and Eta is the NCEP operational mesoscale model.] Only data close to the east coast of the United States are collected, where both the WSI NEXRAD data and the Eta analyses are accurate.

For the subset of data for which WSI NEXRAD detects no rain, within the optimal part of the swath, and for Eta analysis wind speeds between 3 and 20 m s⁻¹, the rms differences between SeaWinds and Eta analysis wind speed and direction are 1.73 m s⁻¹ and 21°, respectively. These rms differences increase significantly whenever WSI NEXRAD detects rain, even light rain. The SeaWinds rain indices are strongly correlated with the WSI NEXRAD precipitation rates. While for high rain rates most winds are correctly flagged, many cases of light rain are not detected.

1. Introduction

The SeaWinds scatterometer on *Midori-2* was launched at 0131 UTC 14 December 2002 from the Tanegashima Space Center in Japan. After an initial checkout period, the scatterometer officially began returning data beginning on 10 April 2003. Unfortunately, the SeaWinds mission ended prematurely on 24 October 2003, when all communication with *Midori-2* ceased. Thus SeaWinds data are available only for a 6.5-month period. An identical instrument is also on the QuikSCAT satellite. [Both instruments are sometimes called SeaWinds. Here both the scatterometer on board QuikSCAT and the satellite itself are referred to as QuikSCAT. SeaWinds used in the singular sense will refer to the *Midori-2* scatterometer. *Midori-2* was known as the Advanced Earth Observing Satellite (ADEOS)-2 prior to launch.] *Midori-2* had nearly the same orbit as QuikSCAT, but with a 2225 local standard time (LST) ascending node time as compared to 0600 LST for QuikSCAT. *Midori-2* also carried the Advanced Microwave Scanning Radiometer (AMSR), a passive microwave instrument, but these data were not yet released at the time of the study.

The focus of this study is an evaluation of SeaWinds wind vector retrievals and operational rain flags in the

presence of rain. Because the quality of the SeaWinds wind retrievals is expected to suffer in the presence of rain, data products from SeaWinds are compared to winds from the Eta analyses and to estimated precipitation from Weather Services International Corporation (WSI). The WSI product we use is based on the U.S. Next Generation Radar (NEXRAD) network of Weather Surveillance Radar-1988 Doppler (WSR-88D) installations. Results are subsetted by wind speed and cross-track position, and SeaWinds' accuracy is evaluated versus observed WSI NEXRAD rain rate and Eta analysis wind speed. The area of study is along the U.S. East Coast (24°–48°N, 64°–84°W) where the Eta analyses are expected to be extremely accurate due to the advection of information from the data-rich analysis just upstream over the continent by prevailing westerlies. Comparisons are restricted to areas close to the coast within the coverage of the NEXRAD system (within the approximately 230-km range of each individual site). The SeaWinds data analyzed here begin with rev 1668 on 10 April 2003 and end with rev 2545 on 10 June 2003. We focus on the 25-km-resolution vector wind estimates and the rain flags contained in the Level 2B data product produced by the Jet Propulsion Laboratory (JPL).

The Eta analysis winds are not error free, and all comparisons are, strictly speaking, differences not errors. However, when rain is detected, the Eta analysis winds can effectively serve as ground truth. As we will show, the Eta analysis winds are remarkably consistent with the scatterometer winds when WSI NEXRAD detects

Corresponding author address: Dr. Ross N. Hoffman, Atmospheric and Environmental Research, Inc., 131 Hartwell Avenue, Lexington, MA 02421-3126.
E-mail: rhoffman@aer.com

no rain. In the presence of rain we expect the scatterometer data to be affected but not the Eta analysis winds. Therefore, the large increases in the mean and standard deviation of the differences in rainy cases are attributed to rain-induced scatterometer errors.

2. Data

a. SeaWinds scatterometer data

The SeaWinds instruments are conically scanning Ku-band scatterometers and are described by Shirliffe (1999). The SeaWinds data are described thoroughly by Lungu (2002). The SeaWinds data processing system produces a dataset during each major phase of processing. All the data needed for this study are contained in the level 2B datasets. The level 2B data elements and data element characteristics of interest to this study are described below.

Scatterometers measure reflected radar energy reported as the normalized radar cross section, denoted σ^0 . Since it is a ratio, σ^0 is unitless and often reported in decibels (dB). Over the ocean, at the 20°–60° incidence angles used, Bragg scattering from centimeter-scale waves on the ocean surface dominates the reflection. These small-scale waves are a response to the surface stress and therefore are closely related to the near-surface wind. Winds are retrieved by matching simulated and actual observations of σ^0 . This is accomplished by minimizing an objective function J , given by

$$J = \sum \frac{(\sigma_o^0 - \sigma_m^0)^2}{\text{var}(\sigma_m^0)}. \quad (1)$$

Here the sum is over all the σ^0 observations within a 25 km \times 25 km cell, subscripts o and m refer to observed and modeled, respectively, and $\text{var}(\sigma_m^0)$ denotes the expected variance of a measurement. The modeled σ^0 and hence J depend on the wind speed (W) and wind direction (D) relative to the antenna pointing direction. The modeled σ^0 also depends on the incidence angle of the observation. The model used to calculate σ_m^0 for the data used here is the so-called QSCAT-1 model function. This model function was derived from a combination of data and theory, using an approach similar to Freilich and Dunbar (1993) and Wentz and Smith (1999).

Because the model function has a nearly harmonic response to wind direction, J has multiple relative minima. Thus the SeaWinds level 2B data contain up to four ambiguous wind vectors (known as ambiguities). These are sorted by increasing values of J . That is, the first, or rank-1, ambiguity best fits the σ^0 data in that wind vector cell (WVC). The second, or rank-2, ambiguity gives the next best fit to the data, and so forth. The negative of J is stored in the datasets as the value of the maximum likelihood estimate. The ambiguity is resolved by a median filter technique (Shaffer et al. 1991). The index of the median filter selection is stored.

The median-filtered selected wind speed and direction are taken to be the “observation” for this study. In the level 2B data, a wind direction is the direction toward which the wind is blowing. This is known as the oceanographic convention. We reverse these directions to agree with the meteorological convention. Alternative observations based on the algorithm of Stiles et al. (2002) are not considered here, although it is expected that statistical results will be fairly similar.

It is known that the presence of rainfall within the three-dimensional volume observed by a Ku-band scatterometer can have a significant effect on the measured σ^0 , and hence the retrieved wind vector. The primary effects are due to scattering and attenuation by the airborne raindrops, as well as changes in the actual sea surface roughness due to the impact of the raindrops on the ocean surface (Tournadre and Quilfen 2003; Mears et al. 2000b). Scattering and attenuation of the scatterometer beam by rain obscures the backscatter signal from the surface. At lower wind speeds the surface signal is smaller and this effect is larger. At higher rain rates σ^0 is dominated by the direct isotropic backscatter from raindrops of the incident radar pulse back to the sensor. Consequently, these observations are interpreted by the scatterometer as winds with anomalously high speeds and in the most contaminated cases with directions perpendicular to the satellite track. Note that significant rain effects have not been reported for scatterometers such as those on the European Remote Sensing Satellites (*ERS-1* and *ERS-2*) that operate in the lower-frequency C band.

In order to detect these rain effects the JPL operational processing system combines several sources of information, including a normalized objective function (Mears et al. 2000a), the retrieved wind speed, the retrieved wind direction relative to the spacecraft track, and the noise-derived brightness temperature (Jones et al. 2000a,b). The method uses a multidimensional histogram (MUDH) (Huddleston and Stiles 2000b) to estimate P_R , the probability of rain of sufficient intensity (≥ 2 km mm h⁻¹) to compromise the wind retrieval. Since MUDH was tuned to (Special Sensor Microwave Imager (SSM/I)) vertically integrated rain rates greater than or equal to 2 km mm h⁻¹, P_R is the probability of rain of that intensity, not the probability of rain occurrence. Here we refer to P_R as the MUDH rain index. If the P_R value exceeds a critical value, then the rain flag is set in the WVC quality flag (Huddleston and Stiles 2000a). For P_R values less than a second critical value the rain flag is then cleared unless corroborated by at least four other preliminary rain flags in a 5 \times 5 neighborhood. The critical values are different for each satellite and are different in the far swath. (See section 3b for a description of the satellite swath.)

The data used in this study were officially released in October 2003, after the SeaWinds calibration phase was completed. Prior to this date, the SeaWinds ground processing was refined and checked, initial postlaunch

σ^0 calibrations were determined, and the radiometer mode for SeaWinds was calibrated to allow an autonomous rain flag to be calculated. The intent was to match SeaWinds performance to that of QuikSCAT. Kellogg et al. (2003) state that the SeaWinds σ^0 measurements were relatively calibrated to those of QuikSCAT to within 0.1 dB using spatially and temporally collocated QuikSCAT and SeaWinds measurements, and both National Centers for Environmental Prediction (NCEP) and European Centre for Medium-Range Weather Forecasts (ECMWF) operational surface analyses.

b. WSI NEXRAD precipitation data

The WSI NEXRAD data used in this study are named the NOWrad SPECIAL precipitation product, which we routinely download and archive in near-real time by a dedicated WSI ground station. These data are produced on a regular $\approx 2 \text{ km} \times 2 \text{ km}$ latitude-longitude grid every 15 min covering the continental United States. Since June 2000, the NOWrad SPECIAL data precision is 0.254 mm (0.01 in.) (M. Pirone 2000, personal communication). The maximum 15-min accumulation allowed by the data format is ≈ 32 mm.

The WSI processing algorithm is described by Grassotti et al. (2003). A hybrid scan is constructed by selecting from among the original NEXRAD three-dimensional reflectivities. These data are quality controlled and then a reflectivity mosaic is created by taking the maximum value from overlapping radars within each 2-km grid box. This is followed by a conversion from reflectivity to rain rate. In the WSI approach the coefficients of the Z - R (reflectivity-rain rate) relationship are stratified by estimates of precipitable water and static stability from the NCEP operational gridded analyses separately for each season and each NEXRAD site. Grassotti et al. (2003) compared the WSI NEXRAD product with operational gauge-adjusted National Oceanic and Atmospheric Administration (NOAA) NEXRAD estimates and rain gauges over the central United States. They found a ≈ 0.6 correlation of WSI NEXRAD and gauge daily rainfall amounts. For hourly data the scatter is greater, but in summer, when precipitating elements are often small, WSI NEXRAD hourly data detect many rain events missed by the gauges.

In addition to using the individual 15-min rainfall analyses, we also calculated the total accumulated rainfall for the 2-month period 1 April-31 May 2003 (see Fig. 1). By accumulating rainfall over this period we are able to clearly see the effects of range fading in the data; by applying a suitable threshold this rainfall map defines the region in which the 15-min rainfall estimates are of relatively high quality. All results presented below in section 5 are for data that have been quality controlled using a mask determined in this way with a critical value of 100 mm.

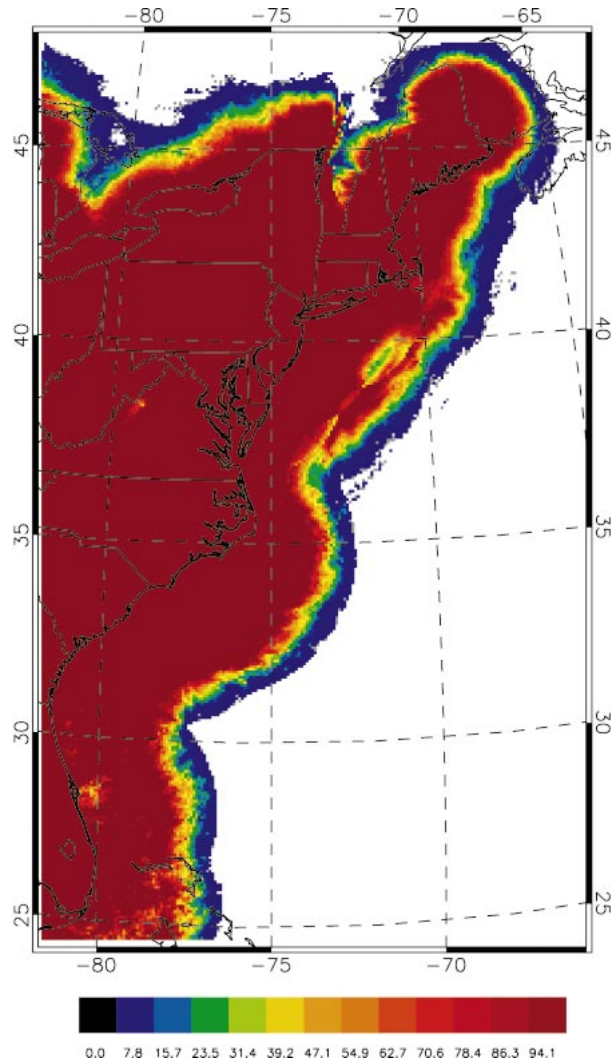


FIG. 1. Accumulated WSI NEXRAD-based rainfall (mm) for the period 1 Apr-31 May 2003 over the eastern United States. The color scale was chosen to saturate at values greater than or equal to 100 mm.

c. NCEP Eta analysis data

The NCEP mesoscale Eta Model is distinguished from other mesoscale models by using a step mountain coordinate system (Black 1994). The Eta Model includes a comprehensive suite of parameterizations of subgrid-scale processes, including a land surface model, convective parameterization, boundary layer model, and cloud parameterization. The Eta 10-m winds used in this study have not been corrected for stability effects. On the other hand, the scatterometer winds are effectively 10-m neutral stability winds measured with respect to ocean currents. Therefore, stability effects and ocean currents, especially the Gulf Stream, are additional sources of difference between the Eta and scatterometer winds.

The Eta data assimilation system (Rogers et al. 1996)

is based on three-dimensional variational analysis. The most current version of the Eta Model and the Eta data assimilation system are described by Rogers et al. (2001a,b). Since November 2001, the Eta data assimilation system uses a 12-km grid that covers the continental United States and surrounding area. The 12-km grid is much better at representing topography and the coastline than previous versions. Modeled winds near the coast should therefore better reflect the effects of local topography. The data are interpolated to the commonly used 40-km Lambert conformal grid known as “Eta 212” for archiving. It is this form of the analyses obtained from the National Center for Atmospheric Research (NCAR) archives that is used here. (Since the 12-km Eta analyses and forecasts are relatively smooth the 40-km grid is adequate for storing these data.)

The Eta data assimilation system does not currently use any scatterometer data directly. The Eta three-dimensional variational analysis uses the 3-h Eta forecast initialized with the previous Eta analysis. Boundary conditions are, however, provided by the global data assimilation system that does assimilate QuikSCAT wind observations. Since information from the boundaries generally propagates along with the synoptic weather features from west to east, the effects of scatterometer data on the Eta analyses along the East Coast will be washed out as these features advance over the U.S. observing network. Thus it is fair to say that the Eta-analyzed winds are independent of scatterometer data.

3. Collocation methodology

To examine the accuracy of the SeaWinds vector wind estimates and rain flags, we collocate SeaWinds level 2B data, WSI NEXRAD precipitation rates, and selected Eta analysis variables. We collect SeaWinds data from 10 April to 10 June 2003 over the study area 24°–48°N, 64°–84°W. For this purpose the WSI NEXRAD and Eta analysis data are interpolated to the WVC time and location as described in section 3a.

The collocated data are then selected for further analysis by subsetting and quality control. Subsetting is based on stratification by Eta analysis wind speed and cross-track position. Quality control makes use of the WSI NEXRAD accumulated rain fall amounts and quality control flags present in the SeaWinds level 2B data.

a. Interpolation methods

The WSI NEXRAD rain-rate mosaic closest in time to the time of SeaWinds data is selected for horizontal averaging from the 2-km-resolution WSI grid to the 25-km SeaWinds WVCs. Time interpolation is not necessary for the WSI NEXRAD data since the data are available every 15 min, and the σ^0 data in a single WVC are collected over a time interval of several minutes. The mean WSI NEXRAD rain rate R is calculated for an 11×11 template centered on the WSI grid point

that is the nearest neighbor of the WVC center. For quality control comparison, the WSI NEXRAD accumulated rain fall amounts are averaged using the same template.

Eta analyses of 10-m wind speed and direction are interpolated linearly in space and in time to the location and time of the WVC. Eta analyses are available 8 times daily (i.e., every 3 h).

b. Quality control and stratification

For the purpose of this study we quality control the data selected for comparison by means of several flags within the level 2B WVC quality flag. First, data are rejected if a “missing value” is indicated for any variable of interest. Second, data are rejected if land or ice is present in the WVC, even though there may be sufficient σ^0 data for wind retrieval. Third, data are rejected if not all expected combinations of σ^0 are present in the WVC (corresponding to the four combinations of inner or outer beam and forward or aft viewing geometries). Normally all four combinations are present in each WVC, except in the far swath that is only observed by the outer beam.

The collocated data are then selected by applying the WSI NEXRAD accumulated precipitation mask. That is, the total accumulated rainfall must be greater than 100 mm to ensure that the WVC is within the useful range of the NEXRAD system. Finally, data may be stratified by wind speed (W), cross-track position, and mean rain rate (R) since validation of previous scatterometers indicate that there are significant variations of accuracy associated with these three variables.

The coarsest stratification of wind speed has categories low, medium, and high. In this study we focus on wind speeds in the range $3 < W \leq 20 \text{ m s}^{-1}$ since the instrument specification calls for highly accurate winds in this particular speed range. Low winds tend to have larger directional errors. At very low wind speeds there are no small-scale waves and thus no Bragg scattering (Shankaranarayanan and Donelan 2001). High winds tend to have large wind speed errors, perhaps because high winds are often associated with sharp gradients, precipitation, and nonsteady conditions (Brown 1983), or because the data available to tune the model function in the high wind regime are limited. At very high winds additional physical processes such as breaking waves, spray, and foam affect backscatter, and even buoy measurements become suspect due to tipping and shadowing of the buoy by large waves (Brown 2000).

The coarsest stratification of cross-track position also has three categories: nadir, optimal, and far swaths. SeaWinds accommodates measurements in a 1900-km-wide swath, centered at nadir. The swath is divided into 76 wind vector cells. The “far” swath or one-beam region is within 225 km of the left and right edges of the swath (i.e., WVC numbers 1–10 and 67–76, respectively). This region is only measured by the outer

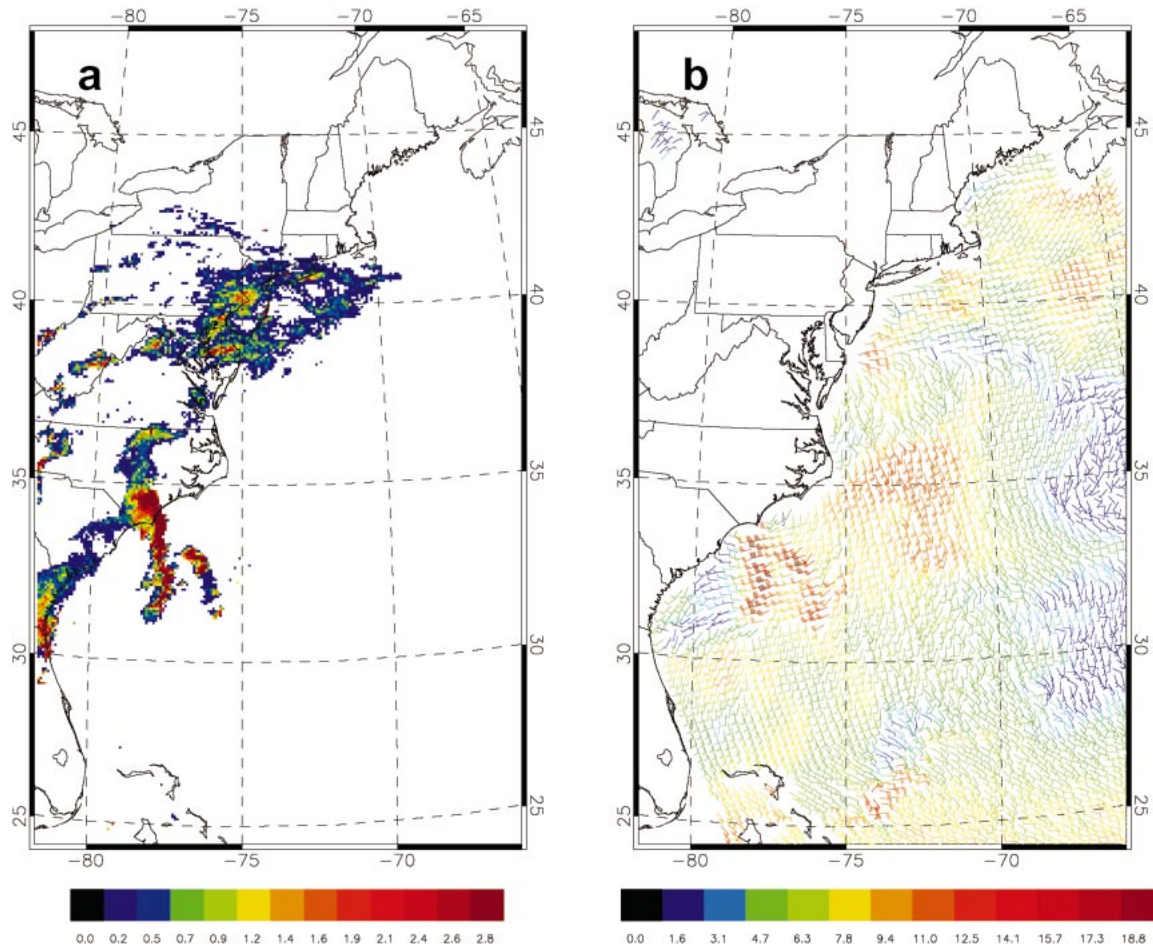


FIG. 2. Collocated WSI NEXRAD and SeaWinds scatterometer data at \approx 0300 UTC 4 Jun 2003. (a) WSI NEXRAD 2 km \times 2 km mosaic of 15-min accumulated rainfall (mm) valid at 0300 UTC 4 Jun 2003. The maximum rainfall amount is 3 mm. (b) SeaWinds wind vectors for rev 2452 valid at 0253 UTC. Barbs indicate wind speed (kt), and colors indicate speed (m s^{-1}). Wind speeds greater than 20 m s^{-1} are plotted in red.

beam. The “nadir” part of the swath (WVC numbers 31–46) is within 200 km of nadir. The “optimal” regions of the swath are between the nadir and far swath regions. The term optimal is used because the azimuthal diversity of σ^0 measurements is near to ideal for sensing wind direction in these regions. (Some authors refer to the optimal swath as the “sweet spot.”) The optimal regions are 500 km wide on the left and right sides of the spacecraft (corresponding to WVC numbers 11–30 and 47–66, respectively).

Azimuthal diversity is lower in the nadir and far swath regions, decreasing toward nadir and the edge of the swath. In this study we will focus on the combined nadir and optimal swath regions where measurements from two beams are available.

4. Synoptic view of rain contamination: Two cases

In this section we present two examples of precipitation-producing systems to show the synoptic manifestation of rain contamination in the SeaWinds winds.

a. 4 June 2003: Coastal storm

At 0300 UTC 4 June 2003, corresponding to SeaWinds rev 2452, precipitation south of New England and east of New Jersey was associated with the warm front of a midlatitude cyclone that was moving into West Virginia. Figure 2a shows the WSI NEXRAD 15-min accumulated rainfall 2 km \times 2 km mosaic at this time, and Fig. 3a shows the WSI NEXRAD data collocated with SeaWinds WVCs for rev 2452. Note that WVCs where the total accumulated rainfall is less than 100 mm (see Fig. 1) are not used in this study and are plotted as open symbols in Fig. 3a.

A surface cold front extended southwest from the cyclone’s center. Well ahead of this front, in the warm sector of the cyclone, an area of convection was moving off the South Carolina coast and into the Atlantic Ocean. A warm front extends through New England. Warm air advection aloft was helping to lift the air ahead of this front. The warm front is seen in the scatterometer wind field by the veering of the wind from easterly off of

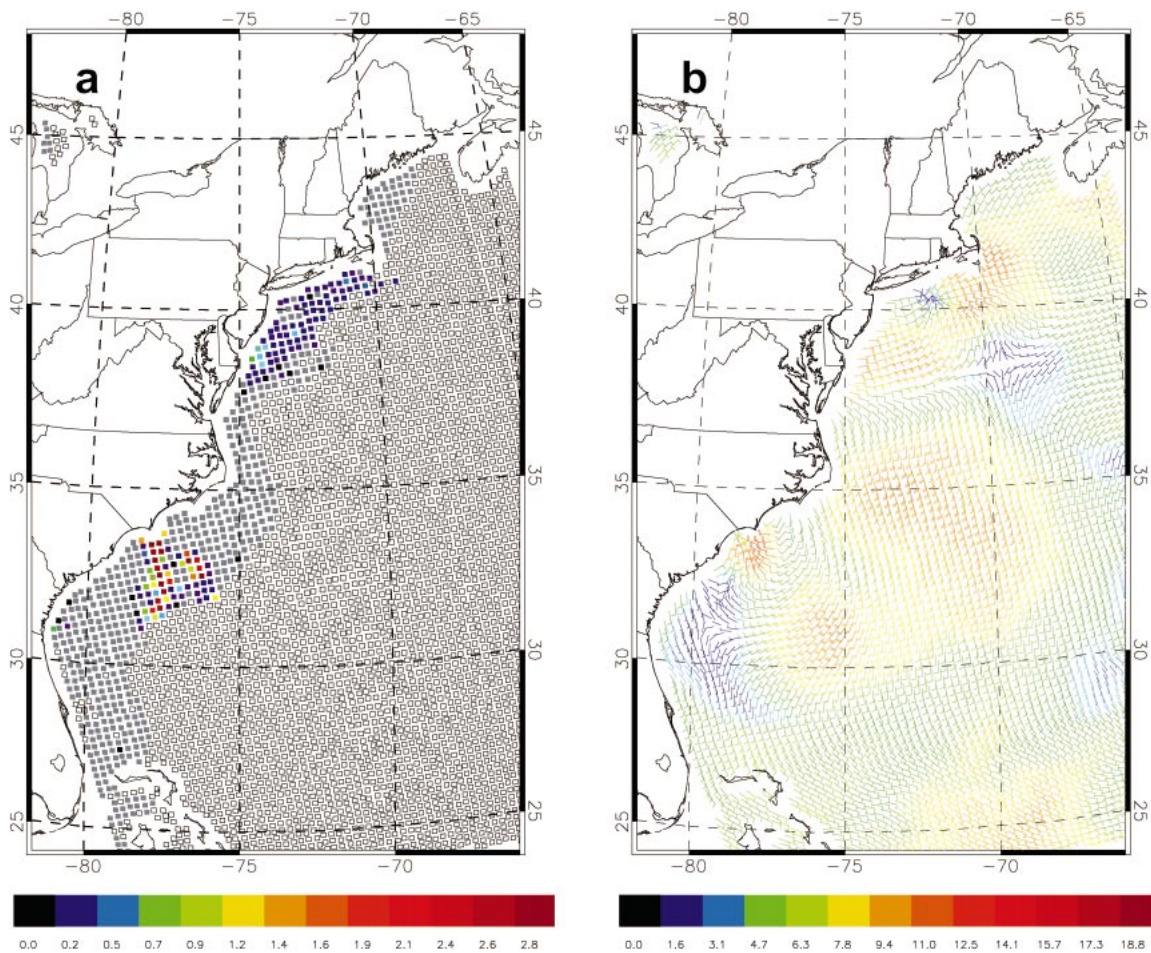


FIG. 3. WSI NEXRAD rainfall and Eta analysis winds collocated with SeaWinds WVCs for rev 2452. (a) WSI rainfall at WVCs plotted with same color scale as in Fig. 2a, except that gray indicates no rain detected. Open symbols indicate WVCs masked out by the total accumulated rainfall mask based on Fig. 1. (b) Eta analysis at WVCs plotted as in Fig. 2b.

New Jersey through southeasterly to southerly off of Virginia (Fig. 2b). Note that the pattern of intense convective precipitation east of South Carolina in the shape of lowercase letter “h” is mirrored in the SeaWinds wind speeds. Typically, high rain rates cause anomalously high wind retrievals because of increased backscattering by raindrops. The effect of rain on scatterometer wind speeds is particularly clear in this case since the Eta wind speeds in the region are light (generally $<10 \text{ m s}^{-1}$) except just offshore of the border between North and South Carolina (Fig. 3b). Comparing Fig. 2b and Fig. 3b we see that the Eta and SeaWinds winds both depict generally southerly winds in the southern part of the domain, a col close to 38°N , 69°W with the aforementioned wind shear front between the col and the Delmarva Peninsula, and an area of divergence close to eastern Long Island, New York, around 41°N , 72°W . While the Eta wind field is much smoother, we suspect that many of the small-scale features in the scatterometer data are present in nature, but that the WVC-to-WVC jitter in the wind directions is probably a manifestation

of sensitivity to noise in the σ^0 measurements. In any case, scales not represented by the smoother Eta wind field, but present in the SeaWinds wind field, will contribute to the difference statistics. These statistics as well as statistics showing the effects of rain on the quality of scatterometer winds are described quantitatively in section 5.

b. 18 September 2003: Hurricane Isabel

At 1600 UTC 18 September 2003, corresponding to SeaWinds rev 3970, Hurricane Isabel was making landfall in the Carolinas. At this time the best track estimate has Isabel’s central pressure below 960 hPa and maximum sustained winds in excess of 85 kt (Beven and Cobb 2004). Figure 4a shows the WSI NEXRAD 15-min accumulated rainfall $2 \text{ km} \times 2 \text{ km}$ mosaic at this time. Figure 4b shows the SeaWinds wind vectors for rev 3970. Note that rain contamination east of South Carolina is evident in wind directions precisely perpendicular to the satellite track in the western part of the

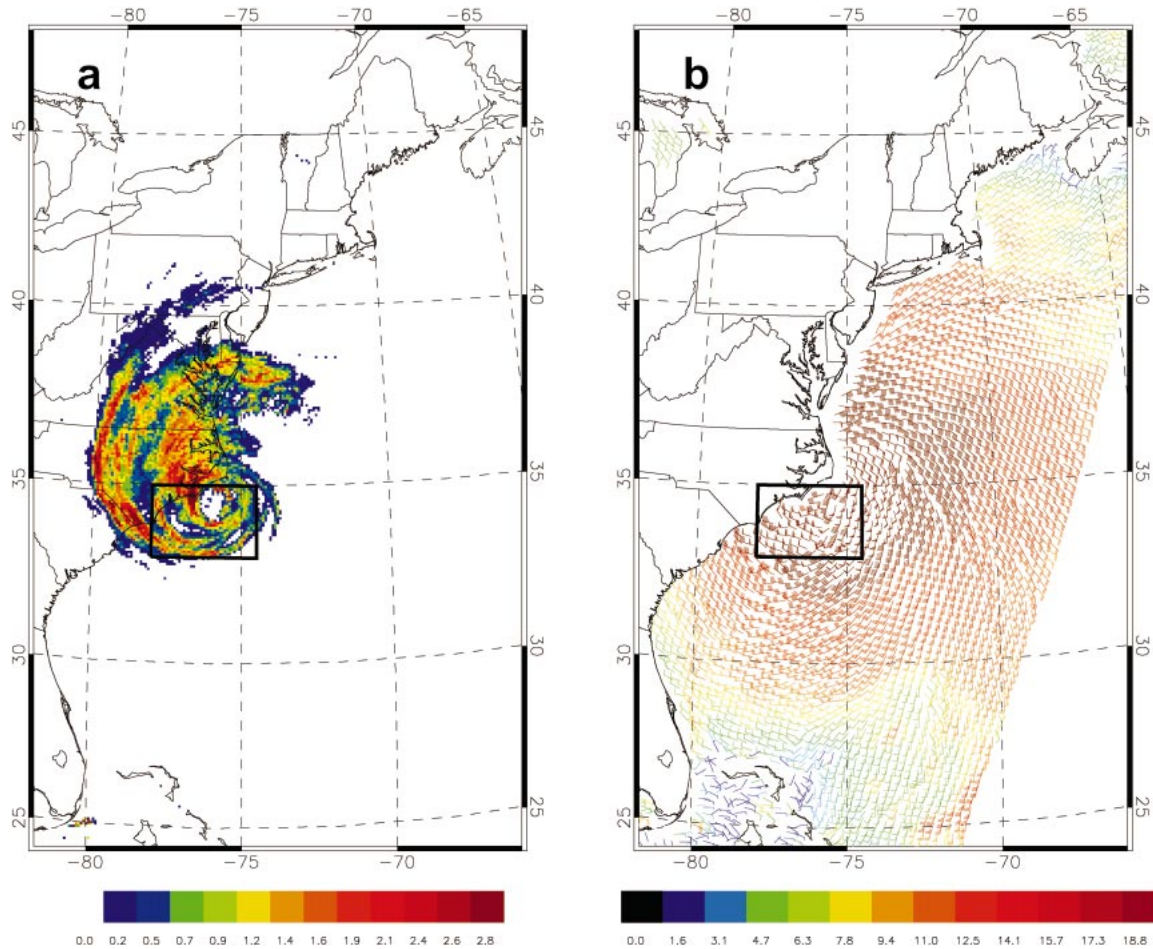


FIG. 4. Collocated WSI NEXRAD and SeaWinds scatterometer data at ≈ 1600 UTC 18 Sep 2003 as Hurricane Isabel was making landfall. (a) WSI NEXRAD $2 \text{ km} \times 2 \text{ km}$ mosaic of 15-min accumulated rainfall (mm) valid at 1600 UTC. The maximum rainfall amount is 3 mm. (b) SeaWinds wind vectors for rev 3970 valid at 1602 UTC. Barbs indicate wind speed (kt), and colors indicate speed (m s^{-1}). Wind speeds greater than 20 m s^{-1} are plotted in red. The rectangular subregion off the Carolinas indicates the area around the hurricane eye that is plotted in Fig. 5.

area marked by rectangles in Fig. 4. Winds perpendicular to the satellite track result from σ^0 measurements being approximately equal for all beams and are likely the result of heavy rain. Figure 5 shows a closeup of the hurricane eye. The white rectangle around each wind vector approximately delineates the $22 \text{ km} \times 22 \text{ km}$ area used to calculate R . Some of the WVCs in the eye are unaffected by rain but may be affected by large waves and foam. Note that all WVCs within $\approx 150 \text{ km}$ of the eye, including all those in Fig. 5, were flagged by MUDH.

5. Statistical results

First we consider the differences between SeaWinds and Eta analysis wind speeds (δW) and wind directions (δD) in the absence of rain contamination. Table 1 contains key wind speed and direction difference statistics (scatterometer minus Eta analysis) for various subsets of the collocated data. The statistics include the sample

size, the mean, the standard deviation, the rms, and the mean absolute difference. The first line is for the “best case,” that is, selecting data when the Eta analysis wind speed is between 3 and 20 m s^{-1} , selecting only the optimal swath, using the ambiguity closest to the Eta analysis, and using WSI NEXRAD to eliminate rainy WVCs. The progression then adds nadir WVCs (line 2 of Table 1), uses the ambiguity selected by the JPL median filter (line 3), selects data for all Eta analysis wind speeds (line 7), selects data for all swath locations (line 8), and, finally, selects all data including rainy WVCs (line 9). For comparison, lines 4 and 6 are similar to line 3, except that line 4 shows results using the MUDH rain flag to identify nonrainy WVCs and line 6 shows results for QuikSCAT. Line 5 contains results when both WSI NEXRAD and MUDH are used to eliminate rainy points, which is a more stringent quality control. Not surprisingly, this line contains the smallest differences, since fewer rainy points are likely to have been included in the sample. The results for line 3 in

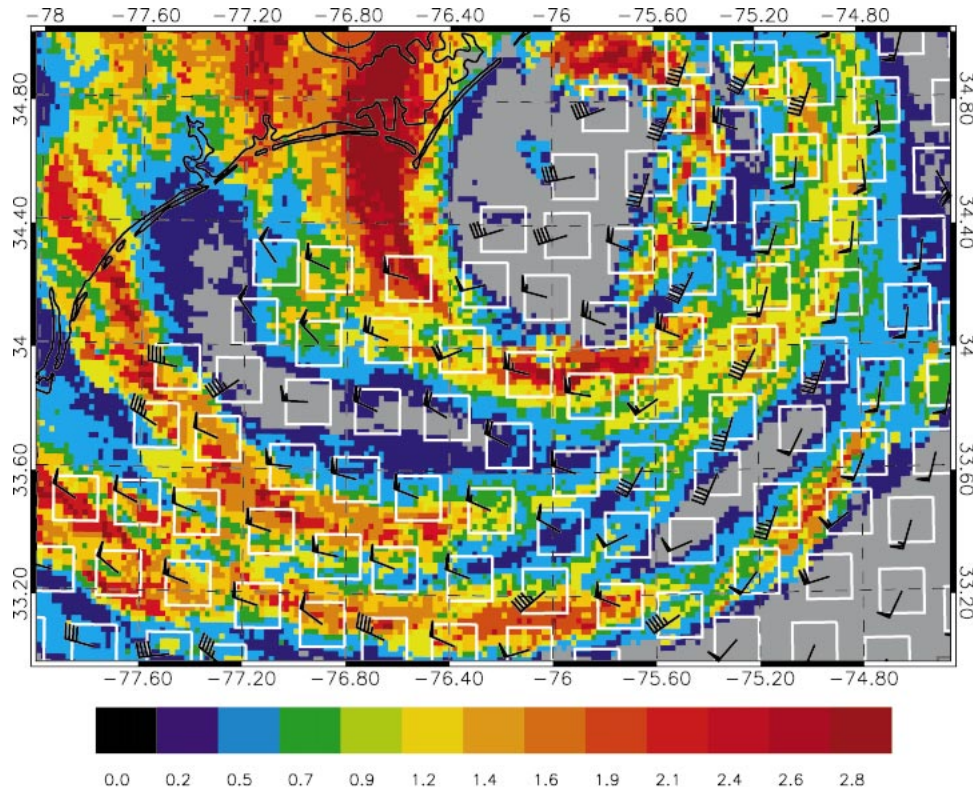


FIG. 5. Region near the eye of Hurricane Isabel showing the WSI NEXRAD rainfall data and the SeaWinds wind vectors from Fig. 4. The white square around each wind vector delineates the approximate area used to calculate R , the mean rain rate in the neighborhood of the WVC center.

the table are printed in bold because they represent the “standard” configuration for which statistics presented in Figs. 7–10 were calculated.

Consider the third line, the case of two-beam median-filtered SeaWinds data, for Eta analysis winds in the 3–20 m s^{-1} speed range and excluding cases with any WSI NEXRAD rain. The wind speed difference standard de-

viation is less than 1.7 m s^{-1} , and the mean absolute direction difference is only 21° . These values demonstrate that the SeaWinds and Eta analysis winds are remarkably consistent. The wind speed bias of $\approx 0.5 \text{ m s}^{-1}$ is likely due in part to the Eta analyses underestimating the true wind. While we are not aware of a published comparison of Eta analyses and buoys to bol-

TABLE 1. Statistics of wind speed difference (δW) and wind direction difference (δD) for scatterometer minus NCEP Eta analysis for subsets of all collocated data, where SD denotes standard deviation and MAD denotes mean absolute difference. The following parameters are varied to produce the subsets: Eta analysis wind speed range (m s^{-1}), region of the SeaWinds swath, ambiguity selection (Amb. sel.) method, and rain quality control (QC) technique. The 3–20 m s^{-1} speed range is specified in defining the instrument requirements. The optimal swath has the greatest diversity of observing incidence and relative azimuth angles. The two-beam swath adds to optimal the nadir region where the relative azimuth angle diversity is low. The Eta ambiguity selection method chooses the ambiguity closest to the Eta analysis; MF refers to the median filter used by JPL. WSI rain quality control eliminates all observations when WSI NEXRAD detects rain and MUDH quality control uses the operation JPL multidimensional histogram rain flag. For reference, line numbers are indicated in the leftmost column. Line 3 in bold corresponds to the subsetting criteria used in Figs. 7–10.

Instrument	Speed range	Swath	Amb. sel.	Rain QC	Sample size	δW (m s^{-1})			δD ($^\circ$)			
						Mean	SD	Rms	Mean	Rms	MAD	
1	SeaWinds	3–20	Optimal	Eta	WSI	29 900	0.49	1.67	1.74	-4	22	16
2	SeaWinds	3–20	Two beam	Eta	WSI	41 549	0.47	1.69	1.75	-3	24	18
3	SeaWinds	3–20	Two beam	MF	WSI	41 549	0.46	1.67	1.73	-4	30	21
4	SeaWinds	3–20	Two beam	MF	MUDH	39 607	0.38	1.57	1.62	-4	30	21
5	SeaWinds	3–20	Two beam	MF	WSI+MUDH	38 150	0.33	1.51	1.55	-4	29	20
6	QuikSCAT	3–20	Two beam	MF	WSI	42 780	0.51	1.87	1.94	-6	32	22
7	SeaWinds	All	Two beam	MF	WSI	50 168	0.60	1.72	1.82	-4	40	26
8	SeaWinds	All	All	MF	WSI	63 126	0.62	1.76	1.87	-4	39	26
9	SeaWinds	All	All	MF	None	69 710	0.99	2.41	2.61	-4	41	27

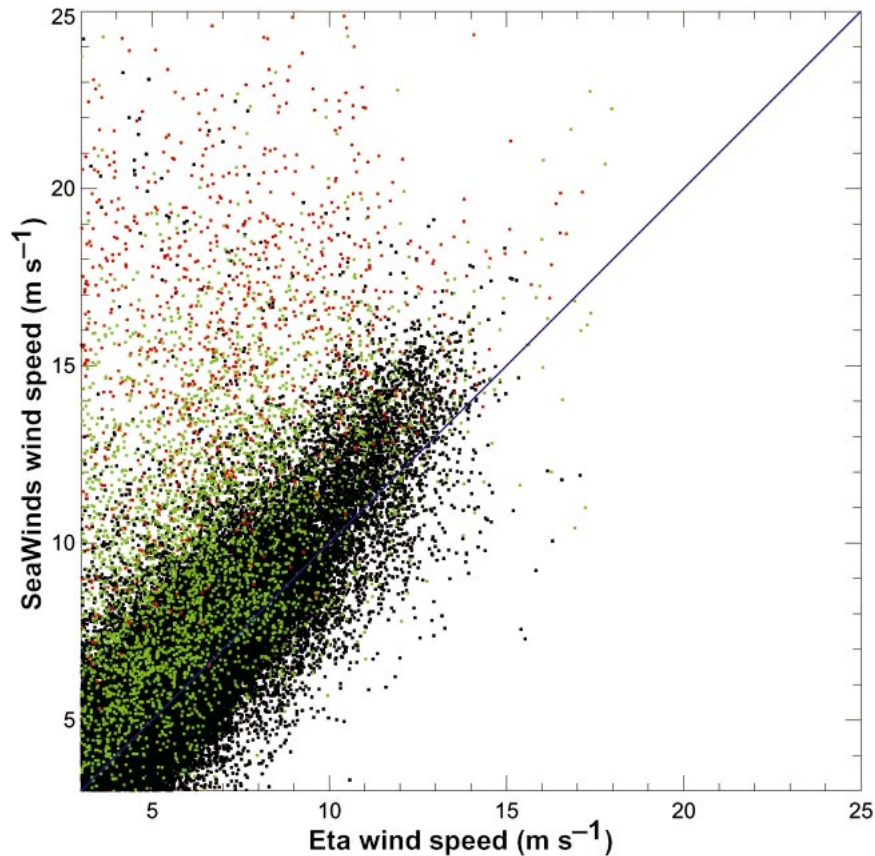


FIG. 6. Scatterplot of SeaWinds vs Eta analysis wind speeds (m s^{-1}). The data subset excludes the outer swath and cases when the NCEP Eta analysis wind speed is less than 3 m s^{-1} or greater than 20 m s^{-1} . Points are plotted in black for cases when no rain is detected by WSI NEXRAD, in green for light rain (up to 2.5 mm h^{-1} reported by WSI NEXRAD), and in red for heavier rain rates.

ster this last assertion, Yu and Gerald (2004) report that the NCEP global data assimilation winds are 0.55 m s^{-1} slower than winds reported by deep water buoys on average.

Note that the bias is smaller for the MUDH quality control and larger when all Eta analysis wind speeds are included. The MUDH rain flag appears to flag observations more aggressively than would be suggested by the WSI NEXRAD data. Note also that the QuikSCAT errors are slightly larger than SeaWinds errors. When WSI NEXRAD detects no rain, we do not see large differences in different parts of the swath. In particular, including the far swath has only a small deleterious effect on the statistics (cf. lines 7 and 8 in the table).

Ambiguity removal errors are probably smaller in the study area than generally because the NCEP global analysis used in the nudging procedure to initialize the median filter should be very accurate off the U.S. East Coast. Even so, the rms wind direction differences for the median-filtered winds are greater than or equal to 29° . The SeaWinds wind directions are just slightly better than QuikSCAT with mean differences of -4.2° ver-

sus -6.0° , respectively. Although small, this difference in direction accuracy is significant at a level of 99%. Wind direction differences increase when all wind speeds are considered. There are very few Eta analysis wind speeds greater than 20 m s^{-1} , so this is due to larger directional errors at low wind speeds.

The collocated wind speeds corresponding to the third line of Table 1 are plotted as black dots in Fig. 6. There is no noticeable trend of the magnitude of the differences with respect to Eta wind speed. The number and distribution of outliers for SeaWinds wind speeds higher than Eta is beyond what one would expect from a normal distribution and may be due to some WVCs contaminated by rain that was not detected by WSI NEXRAD. For comparison, WVCs for which WSI NEXRAD detected light rain or heavier rain are overplotted in green and red, respectively. Clearly, even light rain is very detrimental to the SeaWinds wind speeds.

The larger errors of the rainy data are discussed now. In general, validation statistics are much poorer when WSI NEXRAD detects rain. Key statistics as a function of WSI NEXRAD rain rate are shown in Fig. 7. The figure shows the effect of rain rate on the MUDH rain

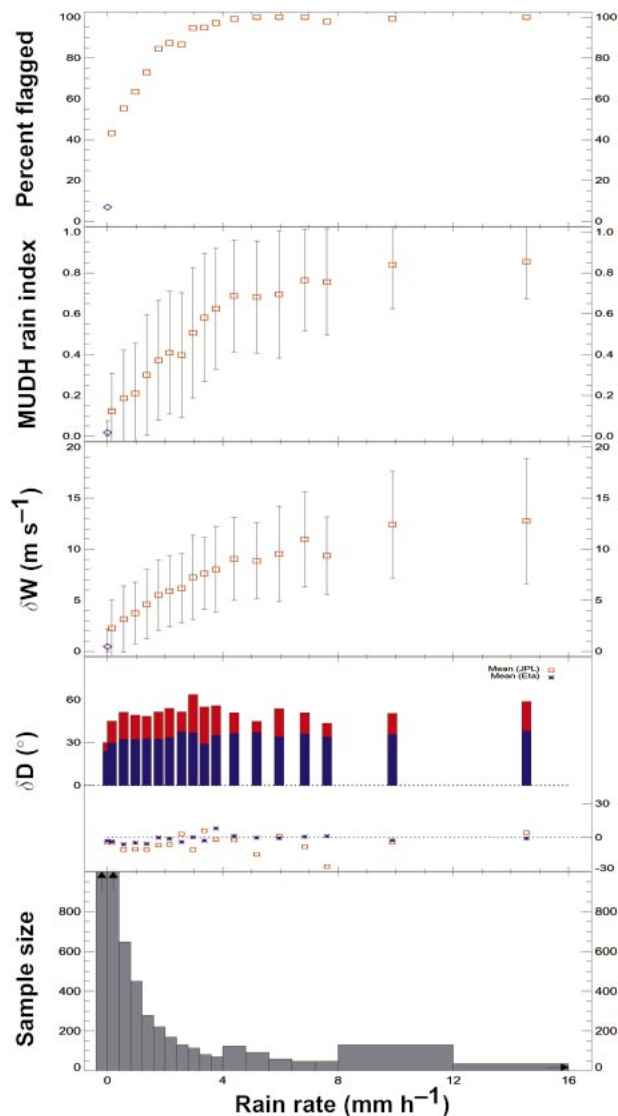


FIG. 7. Validation statistics vs WSI NEXRAD mean rain rate (mm h^{-1}). The data subset excludes the outer swath and cases when the NCEP Eta analysis wind speed is less than 3 m s^{-1} or greater than 20 m s^{-1} . Symbols are plotted at the mean within the bin for both abscissa and ordinate. The first bin or symbol shown is for no rain detected. The percent flagged is according to the operational JPL MUDH rain flag. The MUDH rain index is used to generate these flags. The scatterometer minus analysis wind speed and direction differences are denoted δW and δD . In the MUDH rain index and wind speed difference plots the whiskers show ± 1 std dev. In the wind direction difference plots the std dev of the differences (bars) and mean differences (symbols, scale on right) are shown for the JPL median-filter-selected ambiguity (red) and for the ambiguity closest to the Eta analysis (blue). Sample sizes are shown in lower panel; vertical and horizontal arrows indicate that the actual bar extends beyond the edge of the plot. The first two sample bins contain 41 548 and 1526 WVCs, respectively, and the last sample bin is for all rain rates greater than 12 mm h^{-1} .

flag and rain index (upper two panels) and the wind speed and wind direction difference statistics (next three panels). Increases in the difference statistics when it is rainy relative to the no-rain case is attributed to increased errors in the scatterometer data here.

The bottom panel is a barplot showing the widths of the bins and the sample sizes. In this panel vertical and horizontal arrows indicate that the actual bar extends beyond the edge of the plot. In the figure the first bin is for no rain detected, the second bin is for $0 < R \leq 0.04 \text{ mm h}^{-1}$, and so forth. (The first bin is arbitrarily set to the same thickness as the second bin.) In the other panels symbols are plotted at the mean rain rate in each bin.

The top panel in the figure shows the percent flagged by MUDH. Red squares show that the probability of detection increases with increasing rain rate. The blue diamond plotted for zero WSI NEXRAD rain rate gives the percentage of false alarms raised for the no-rain cases. (Probability of detection and false alarm are here defined taking the WSI NEXRAD detection of rain as the truth. Probability of detection is defined as the number of correctly flagged rainy WVCs divided by the number of rainy WVCs.) Note that the probability of detection of very light rain rates is poor, but moderate and heavy rain are reliably detected. The second panel shows the relationship between the MUDH rain index (P_R) and the WSI NEXRAD rain rate (R). Clearly P_R tends to increase with R in the range $R < 4 \text{ mm h}^{-1}$.

The third panel shows the wind speed difference (δW) statistics, with means as symbols and standard deviations as whiskers. The wind speed bias increases with rain rate, and there is a noticeable jump for even the smallest amount of rain. The wind speed difference standard deviation also increases with rain rate at least up to a rate of 4 mm h^{-1} .

The fourth and fifth panels show the wind direction difference (δD) standard deviations and means for the two methods of ambiguity selection. The standard deviations (means) are shown as red bars (squares) for the median filter selection and blue bars (asterisks) for the closest to Eta analysis selection. The mean wind direction biases are generally negligible, with larger values corresponding to smaller samples. Ambiguity removal errors are considerably larger, especially for the median filter for the rainy cases (45° versus 30°). There is no particular trend with rain rate, but any rain at all has a significant effect on the standard deviation of wind direction differences.

Wind speed differences depend on the actual wind speed and the rain rate because for low speeds the backscatter from the surface is smaller and more easily obscured by rain. Even though the sample sizes are small for high rain rates, this correlation is clear, as demonstrated in Fig. 8. Further analysis (not shown) indicates that for a given mean rain rate, wind speed differences are larger in WVCs with a higher spatial variance of

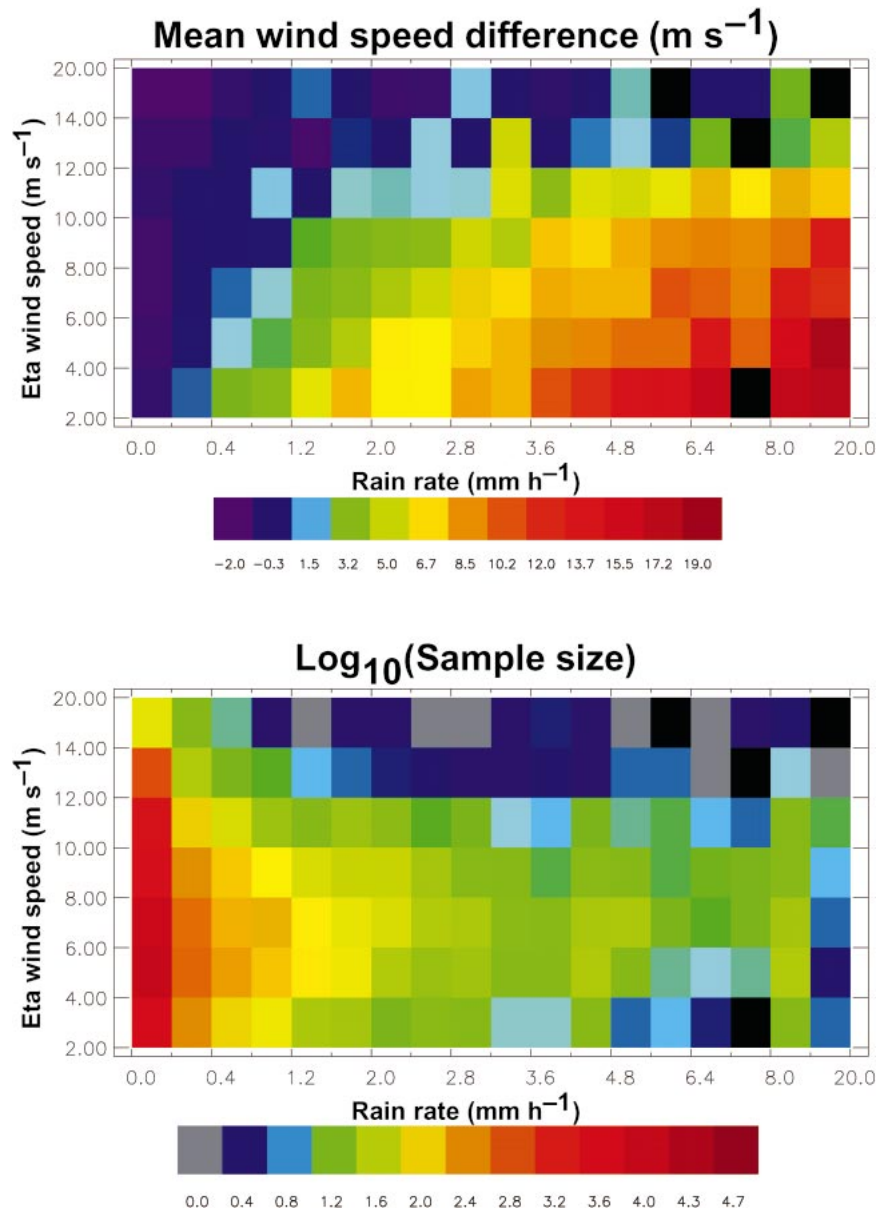


FIG. 8. Mean wind speed difference [SeaWinds minus Eta analysis (m s^{-1})] as a function of WSI NEXRAD rain rate and Eta analysis wind speed. Log_{10} of sample sizes are shown in lower panel. Bins with only one observation are gray, and those with no observations are black.

rain rate. Although the small sample sizes limit the conclusions we can draw, it does imply that wind speed errors are sensitive to the spatial distribution of rainfall within a WVC; one or two heavier rain elements within a WVC may degrade the wind retrieval more than a uniform field of lighter rainfall.

We also find that the MUDH rain flag eliminates many high wind speed WVCs. This is noticeable for Eta analysis wind speeds greater than 10 m s^{-1} (Fig. 9). This suggests that the MUDH P_R gives too much weight to high SeaWinds wind speeds. Of course, high SeaWinds

wind speeds are often caused by rain. Figure 10 shows a clear quasi-linear relationship between the MUDH P_R and wind speed bias. In fact, operational use of data from SeaWinds on QuikSCAT includes a wind speed bias correction that is dependent on the value of P_R (H. Hersbach, ECMWF, 2003, personal communication). Note that in Fig. 10 the operational SeaWinds two-beam threshold values of the MUDH rain-flag spatial filter bound the third sample bin. Thus all samples to the right are flagged, no samples to the left are flagged, and 60% of the third bin are flagged.

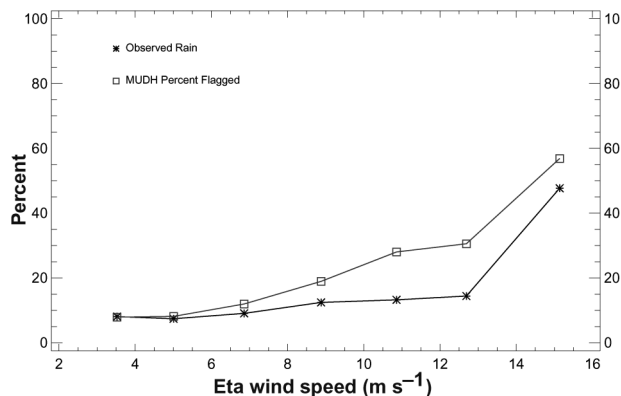


FIG. 9. Percent rain detected by WSI NEXRAD (black asterisk) and flagged by MUDH (blue square) binned by Eta analysis wind speed. Symbols are plotted at the mean within the bin for both abscissa and ordinate. The bin boundaries are every 2 m s⁻¹ starting at 2 m s⁻¹. The last bin for Eta analysis wind speeds greater than 14 m s⁻¹ contains only 109 cases. The other bin sample counts are 6922, 16 047, 12 799, 5735, 2725, and 818 from low to high wind speed.

6. Summary and discussion

To validate the SeaWinds wind data and rain flags we collocate SeaWinds level 2B data, WSI NEXRAD precipitation rates, and Eta analyses for a 2-month period. We only use data close to the U.S. East Coast, where both the NEXRAD data and the Eta analyses are accurate. There are two critical assumptions in using this methodology: first, that the Eta analyses are accurate and, second, that we know the maximum distance from land within which the ground-based radar rainfall estimates are accurate. These assumptions are well supported by a priori arguments and by the consistency of the very good comparisons between Eta analysis and scatterometer winds when WSI NEXRAD is indicating no rain.

The main conclusions of this study are the following.

- 1) SeaWinds and QuikSCAT data have similar characteristics, according to our analysis. SeaWinds appears slightly more accurate than QuikSCAT for rain-free conditions. QuikSCAT rms wind speed differences appear to be about 12% higher than SeaWinds during the study period. All analyses done for SeaWinds were also done for QuikSCAT but are not reported here because the results are so similar.
- 2) The SeaWinds and Eta analysis agreement is excellent: 0.5 m s⁻¹ bias, 1.7 m s⁻¹ standard deviation, and 22° rms difference for the “best” data (i.e., the first line in Table 1).
- 3) We find a significant degradation of the SeaWinds retrieved wind speeds and directions whenever rain is reported by WSI NEXRAD (Fig. 7). This is also true when the MUDH rain flag is set.
- 4) The probability of detection of the operational MUDH rain flag is quite good for moderate and heavy rain: more than 90% of rain events are flagged when the mean rain rate is at least 3 mm h⁻¹. How-

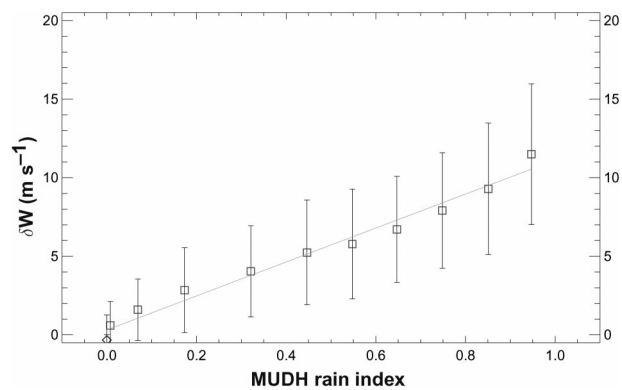


FIG. 10. Wind speed difference [SeaWinds minus Eta analysis (m s⁻¹)] statistics as a function of the MUDH rain index. Symbols are plotted at the mean within the bin for both abscissa and ordinate. The whiskers show ±1 std dev. The first bin or symbol shown is for no rain detected. A linear fit is shown through the bin averages. Sample sizes for low to high rain index are 9837, 29 163, 3027, 1561, 648, 309, 254, 191, 191, 237, and 362.

- ever, for lighter rain events the rain-flag performance degrades, with a probability of detection of less than 50% when the rain rate is below 1 mm h⁻¹ (Fig. 7).
- 5) The MUDH algorithm flags a greater percentage of WVCs than observed in the WSI NEXRAD data at higher wind speeds, especially for wind speeds greater than 8 m s⁻¹ (Fig. 9).
 - 6) Regarding the sensitivity to rainfall, we find a clear quasi-linear relationship between the MUDH rain index and SeaWinds–Eta analysis mean speed differences (Fig. 10).

The significant effect of small rain amounts is surprising and may have important implications for some users of these data, since a high proportion of light rain is not detected. Due to quantization in the WSI NEXRAD data (rain amounts are archived at increments of 0.254 mm for 15-min accumulations), a nonzero mean rain rate R implies that at least one 2 km × 2 km cell in the averaging template has a rain rate of 0.254 mm accumulated in 15 min (or equivalently ≈1 mm h⁻¹). In our analysis the first rainy bin contains WVCs with mean rain rates greater than 0 and less than 0.4 mm h⁻¹. Therefore, this bin would have WVCs containing no more than 40% coverage by such 2 km × 2 km cells (or the equivalent). Yet such a small amount of rain has a distinct effect on the quality of the wind data (e.g., the wind speed bias increases from less than 0.5 m s⁻¹ to more than 2 m s⁻¹). Therefore, an improved rain flag would substantially improve SeaWinds performance because errors are significantly larger even for light rain (1–2 mm h⁻¹), and these light rain rates are not detected reliably. Alternatively, a combined wind and rain retrieval algorithm using SeaWinds data alone may have improved performance under these conditions (Yueh et al. 2003; Draper and Long 2004). Until the rain flag is improved, an alternative is to use the MUDH rain index along with a stricter user-specified threshold (Huddles-

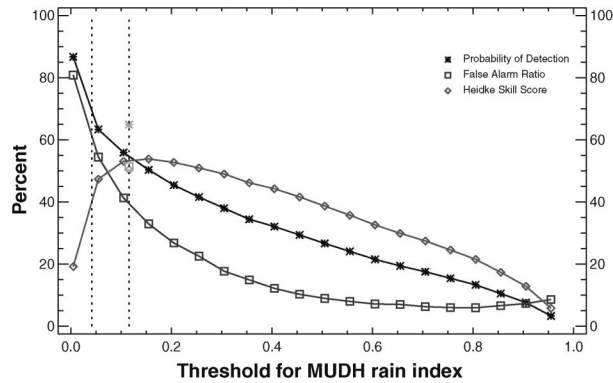


FIG. 11. Skill of MUDH rain flag as a function of the threshold applied to the MUDH rain index. The MUDH rain flag used here is based on a simple threshold without any spatial filtering. A black asterisk is plotted for the probability of detection; a blue square for the false alarm ratio; and a red diamond for the Heidke skill score. The first point plotted is for a very small positive threshold. For reference the two critical thresholds used by the JPL operational MUDH rain flag are denoted by the vertical dotted lines, and the scores for this rain flag are plotted in green symbols at the second of these thresholds.

ton and Stiles 2000a). Figure 11 shows how varying the threshold affects the probability of detection, false alarm ratio, and Heidke skill score of the MUDH rain flag for detecting the occurrence of rain in the WSI NEXRAD data. However, increasing the probability of detection will also increase the false alarm ratio with this approach.

With the premature end of *Midori-2* mission, there will be no new SeaWinds data. Nevertheless, we expect that the results shown here, and the high quality data that have already been obtained, will provide researchers with an opportunity to improve rain detection/correction approaches, especially once the AMSR data are analyzed. These will prove beneficial to future spaceborne scatterometer missions and to the continuing QuikSCAT mission.

Acknowledgments. Data used in the research reported here were provided by the Jet Propulsion Laboratory (JPL) Physical Oceanography Distributed Active Archive Center (PO.DAAC), the National Center for Environmental Prediction (NCEP) through the National Center for Atmospheric Research (NCAR), and Weather Services International Corporation (WSI). We also thank J. Henderson for valuable assistance. Comments of anonymous reviewers helped to improve this paper. This research was supported by the NASA scatterometer project through the Ocean Wind Vector Science Team (OWVST).

REFERENCES

- Beven, J., and H. Cobb, 2004: Tropical cyclone report, Hurricane Isabel, 6–19 September 2003. National Hurricane Center Tech. Rep., 24 pp. [Available online at <http://www.nhc.noaa.gov/2003isabel.shtml>.]
- Black, T. L., 1994: The new NMC mesoscale Eta model: Description and forecast examples. *Wea. Forecasting*, **9**, 265–278.
- Brown, R. A., 1983: On a satellite scatterometer as an anemometer. *J. Geophys. Res.*, **88**, 1663–1673.
- , 2000: On satellite scatterometer model functions. *J. Geophys. Res.*, **105**, 29 195–29 205.
- Draper, D. W., and D. G. Long, 2004: Simultaneous Wind and Rain Retrieval Using SeaWinds Data. *IEEE Trans. Geosci. Remote Sens.*, **42**, 1411–1423.
- Freilich, M. H., and R. S. Dunbar, 1993: Derivation of satellite wind model functions using operational surface wind analyses: An altimeter example. *J. Geophys. Res.*, **98**, 14 633–14 649.
- Grassotti, C., R. N. Hoffman, E. R. Vivoni, and D. Entekhabi, 2003: Multiple timescale intercomparison of two radar products and rain gauge observations over the Arkansas–Red River Basin. *Wea. Forecasting*, **18**, 1207–1229.
- Huddleston, J. N., and B. W. Stiles, 2000a: Multidimensional histogram (MUDH) rain flag. Product description, Version 2.1, Jet Propulsion Laboratory, Pasadena, CA, 8 pp.
- , and —, 2000b: A multidimensional histogram rain-flagging technique for SeaWinds on QuikSCAT. *Proc. Int. Geoscience and Remote Sensing Symp. (IGARSS)*, Honolulu, HI, IEEE, 1232–1234.
- Jones, W. L., R. Meher Shahi, J. Zec, and D. G. Long, 2000a: SeaWinds on QuikSCAT radiometric measurements and calibration. *Proc. Int. Geoscience and Remote Sensing Symp. (IGARSS)*, Honolulu, HI, IEEE, 1027–1029.
- , M. Susanj, J. Zec, and J.-D. Park, 2000b: Validation of QuikSCAT radiometric estimates of rain rate. *Proc. Int. Geoscience and Remote Sensing Symp. (IGARSS)*, Honolulu, HI, IEEE, 1229–1231.
- Kellogg, K., M. H. Freilich, and W. T. Liu, 2003: SeaWinds data release notes. Jet Propulsion Laboratory, Pasadena, CA, 7 pp.
- Lungu, T., 2002: SeaWinds science data product user's manual, overview and geophysical data products. Version 1.0, Jet Propulsion Laboratory, Pasadena, CA, JPL D-21551, 128 pp.
- Mears, C., D. Smith, and F. Wentz, 2000a: Detecting rain with QuikSCAT. *Proc. Int. Geoscience and Remote Sensing Symp. (IGARSS)*, Honolulu, HI, IEEE, 1235–1237.
- , F. Wentz, and D. Smith, 2000b: SeaWinds on QuikSCAT normalized objective function rain flag. Version 1.2, Remote Sensing Systems, Santa Rosa, CA, 13 pp.
- Rogers, E., T. L. Black, D. G. Deaven, G. J. DiMego, Q. Zao, M. Baldwin, and Y. Lin, 1996: Changes to the operational “early” Eta analysis/forecast system at the National Centers for Environmental Prediction. *Wea. Forecasting*, **11**, 391–413.
- , —, B. Ferrier, Y. Lin, D. Parrish, and G. DiMego, 2001a: Changes to the NCEP meso Eta analysis and forecast system: Increase in resolution, new cloud microphysics, modified precipitation assimilation, modified 3DVAR analysis. Technical Procedures Bulletin 488, NWS, Silver Spring, MD, 20 pp. [Available online at <http://www.emc.ncep.noaa.gov/mmb/mmbpl/eta12tpb/> or from the National Weather Service, Office of Meteorology, 1325 East–West Highway, Silver Spring, MD 20910.]
- , M. Ek, Y. L. K. Mitchell, D. Parrish, and G. DiMego, 2001b: Changes to the NCEP meso Eta analysis and forecast system: Assimilation of observed precipitation, upgrades to land-surface physics, modified 3DVAR analysis. Technical Procedures Bulletin 479, NWS, Silver Spring, MD, 13 pp. [Available online at <http://www.emc.ncep.noaa.gov/mmb/mmbpl/spring2001/tpb/> or from the National Weather Service, Office of Meteorology, 1325 East–West Highway, Silver Spring, MD 20910.]
- Shaffer, S. J., R. S. Dunbar, S. V. Hsiao, and D. G. Long, 1991: A median-filter-based ambiguity removal algorithm for NSCAT. *IEEE Trans. Geosci. Remote Sens.*, **29**, 167–174.
- Shankaranarayanan, K., and M. A. Donelan, 2001: A probabilistic approach to scatterometer model function verification. *J. Geophys. Res.*, **106**, 19 969–19 990.
- Shirtilffe, G. M., 1999: QuikSCAT science data product user's man-

- ual, overview and geophysical data products. Version 1.0, Jet Propulsion Laboratory, Pasadena, CA, JPL D-18053, 90 pp.
- Stiles, B. W., B. D. Pollard, and R. S. Dunbar, 2002: Direction interval retrieval with thresholded nudging: A method for improving the accuracy of QuikSCAT winds. *IEEE Trans. Geosci. Remote Sens.*, **40**, 79–89.
- Tournadre, J., and Y. Quilfen, 2003: Impact of rain cell on scatterometer data: 1. Theory and modeling. *J. Geophys. Res.*, **108**, 3225, doi:10.1029/2002JC001428.
- Wentz, F. J., and D. K. Smith, 1999: A model function for the ocean-normalized radar cross section at 14 GHz derived from NSCAT observations. *J. Geophys. Res.*, **104**, 11 499–11 514.
- Yu, T.-W., and V. M. Gerald, 2004: Evaluation of NCEP operational model forecasts of surface wind and pressure fields over the oceans. Preprints, *20th Conf. on Weather Analysis and Forecasting/16th Conf. on Numerical Weather Prediction*, Seattle, WA, Amer. Meteor. Soc., CD-ROM, P4.18.
- Yueh, S. H., B. W. Stiles, and W. T. Liu, 2003: QuikSCAT wind retrievals for tropical cyclones. *IEEE Trans. Geosci. Remote Sens.*, **41**, 2616–2628.